

See discussions, stats, and author profiles for this publication at: <https://www.researchgate.net/publication/279201225>

# Large-Size CH<sub>3</sub>NH<sub>3</sub>PbBr<sub>3</sub> Single Crystal: Growth and In Situ Characterization of the Photophysics Properties

ARTICLE in JOURNAL OF PHYSICAL CHEMISTRY LETTERS · JUNE 2015

Impact Factor: 7.46 · DOI: 10.1021/acs.jpclett.5b01017

---

CITATION

1

READS

192

## 7 AUTHORS, INCLUDING:



Pengjun Zhao

Sungkyunkwan University

33 PUBLICATIONS 105 CITATIONS

[SEE PROFILE](#)



Jinbao Xu

Chinese Academy of Sciences

47 PUBLICATIONS 302 CITATIONS

[SEE PROFILE](#)



Wei Ren

Chinese Academy of Sciences

11 PUBLICATIONS 10 CITATIONS

[SEE PROFILE](#)



Liang Bian

Chinese Academy of Sciences

47 PUBLICATIONS 118 CITATIONS

[SEE PROFILE](#)

## Large-Size $\text{CH}_3\text{NH}_3\text{PbBr}_3$ Single Crystal: Growth and In Situ Characterization of the Photophysics Properties

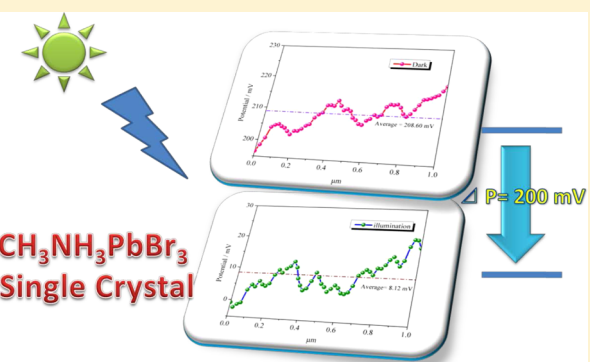
Pengjun Zhao,<sup>†,‡</sup> Jinbao Xu,<sup>\*,†</sup> Xiaoyu Dong,<sup>†</sup> Lei Wang,<sup>†</sup> Wei Ren,<sup>\*,†</sup> Liang Bian,<sup>†</sup> and Aimin Chang<sup>†</sup>

<sup>†</sup>Key Laboratory of Functional Materials and Devices for Special Environments and Xinjiang Key Laboratory of Electronic Information Materials and Devices, Xinjiang Technical Institute of Physics and Chemistry, Chinese Academy of Sciences, Urumqi 830011, PR China

<sup>‡</sup>University of Chinese Academy of Sciences, Beijing 100049, PR China

### Supporting Information

**ABSTRACT:** We reported a facile single-solution fabrication method to grow large-scale  $\text{CH}_3\text{NH}_3\text{PbBr}_3$  hybrid perovskite single crystal at room temperature. The obtained single crystal in this experiment was  $14 \times 14$  mm. The sample's in situ photophysics properties under dark and illumination, including the surface morphology, work function, surface current distribution, microscopic  $I-V$  curves, as well as the polarization behavior, were in situ characterized by integrated utilization of a scanning probe microscopy, respectively. Piezoresponse force microscopy (PFM) phase angles indicated the existence of "polarization" in  $\text{CH}_3\text{NH}_3\text{PbBr}_3$  lattice. Interestingly, the "polarization effect" was enhanced by the plus light source. Moreover, a surface potential shift as large as 200 mV was observed under the condition of the illumination on and off. This research is proposed to provide an opportunity to take a fresh look at the architectural design and photovoltaic performance origin of the hybrid perovskite solar cells.



Recently, a rapid breakthrough in the field of photovoltaic conversion devices has drawn the attention of the world, namely, perovskite solar cells (PSCs). With the introduction of the inorganic–organic hybrid halide perovskite compounds as light harvester, photoelectric conversion efficiency of PSCs has achieved 20%.<sup>1–5</sup> Some superiorities, such as high charge-carrier mobilities, low temperature (below 150 °C) solution process, extreme large carrier diffusion lengths, as well as the outstanding photovoltaic efficiencies, make the PSCs the most promising next-generation solar cells.<sup>6–9</sup>

The chemical formula of hybrid halide perovskite materials can be expressed as  $\text{ABX}_3$ , where A is a monovalence organic cation, usually the methylammonium (MA) or formamidinium (FA) group; B is a bivalent metal cation,  $\text{Pb}^{2+}$  or  $\text{Sn}^{2+}$ ; X is halide ion,  $\text{Cl}^-$ ,  $\text{Br}^-$ , or  $\text{I}^-$ .<sup>10–14</sup> The positively charged organic cation locates at the interstice of a metal-halogen octahedral  $[\text{BX}_6]$  cages.

Currently, there are two common architectural styles of hybrid perovskite in the solar cell devices: planar construction and mesoporous structure.<sup>15–18</sup> Both architectures are made up of hybrid perovskite crystalline grains with several hundred nanometers. As is known, grain boundaries exist in polycrystalline systems, which are carrier recombination centers to trap photogenerated hole and electron pairs.

Most recently, some dramatic research has focused on the properties of large-scale single crystal hybrid halide perovskites. Nie et al. developed a solution-based hot-casting technique to

grow continuous, pinhole-free thin films of organometallic perovskites with millimeter-scale crystalline grains. The fabricated planar structure PSCs exhibited high efficiencies approaching 18%, compared with 9.1% with small grain cells. In addition, performance consistency of PSCs was enhanced when grain became larger.<sup>19</sup> Shi<sup>20</sup> grew sizable crack-free  $\text{MAPbBr}_3$

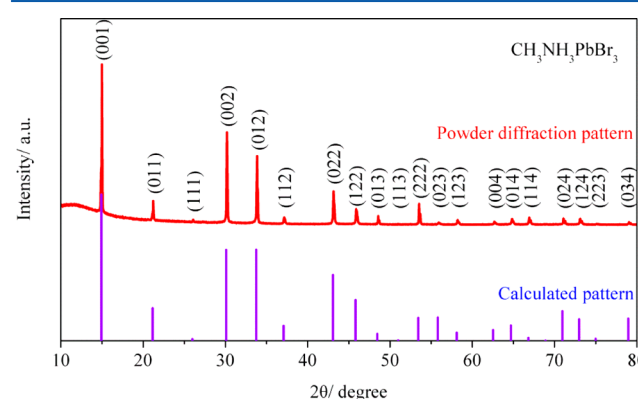


**Figure 1.** Experimental and calculated powder diffraction patterns of  $\text{CH}_3\text{NH}_3\text{PbBr}_3$ .

**Received:** May 16, 2015

**Accepted:** June 18, 2015

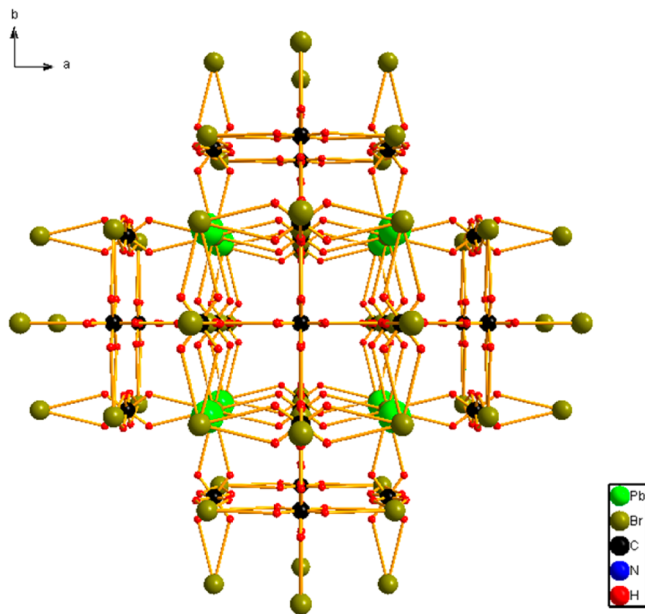


**Figure 2.** View of the lattice structure of  $\text{CH}_3\text{NH}_3\text{PbBr}_3$  along the  $c$  axis.

and  $\text{MAPbI}_3$  single crystals with large volumes over 100 cubic millimeters through an antisolvent vapor-assisted crystallization approach. They observed exceptionally low trap-state densities on the order of  $10^9$  to  $10^{10}$  per cubic centimeter in these single crystals and charge-carrier diffusion lengths exceeding  $10 \mu\text{m}$ , which is ten times larger than that of polycrystalline films. Even more intriguing, Dong<sup>21</sup> reported that the diffusion lengths in  $\text{CH}_3\text{NH}_3\text{PbI}_3$  single crystals could exceed  $175 \mu\text{m}$  under 1 sun illumination and exceed 3 mm under 0.003% sun irradiation. The internal quantum efficiencies approach 100% in thick single-crystal perovskite solar cells. They believed that the long diffusion lengths resulted from greater carrier mobility, lifetime, and dramatically smaller trap densities in the single crystals than polycrystalline thin films.

As a consequence, there is no doubt that intensive investigation of large-scale hybrid perovskite single crystals, including the crystal growth process and photophysical properties, would lead the PSCs to a higher level; however, on the basis of the present literature, research on the growth method of large-scale hybrid perovskite single crystal is relatively rare.<sup>22,23</sup>

We reported a simple synthesis method to fabricate large-scale  $\text{CH}_3\text{NH}_3\text{PbBr}_3$  single crystal via single-solution method at

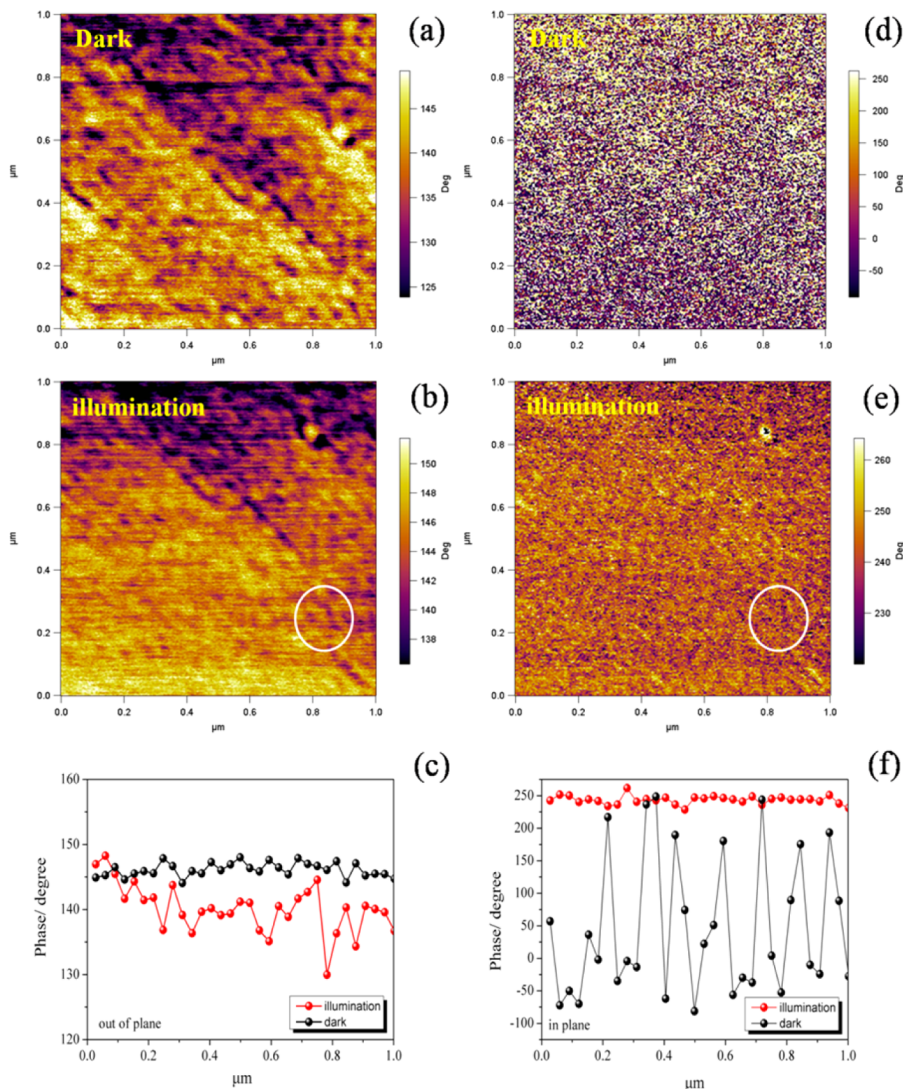


**Figure 3.** OPP (a,b) and IPP (d,e) PFM phase images of  $\text{CH}_3\text{NH}_3\text{PbBr}_3$  single crystal under dark and illumination. (c,f) Corresponding data curves. The white circles in panels b and e mark the domain area.

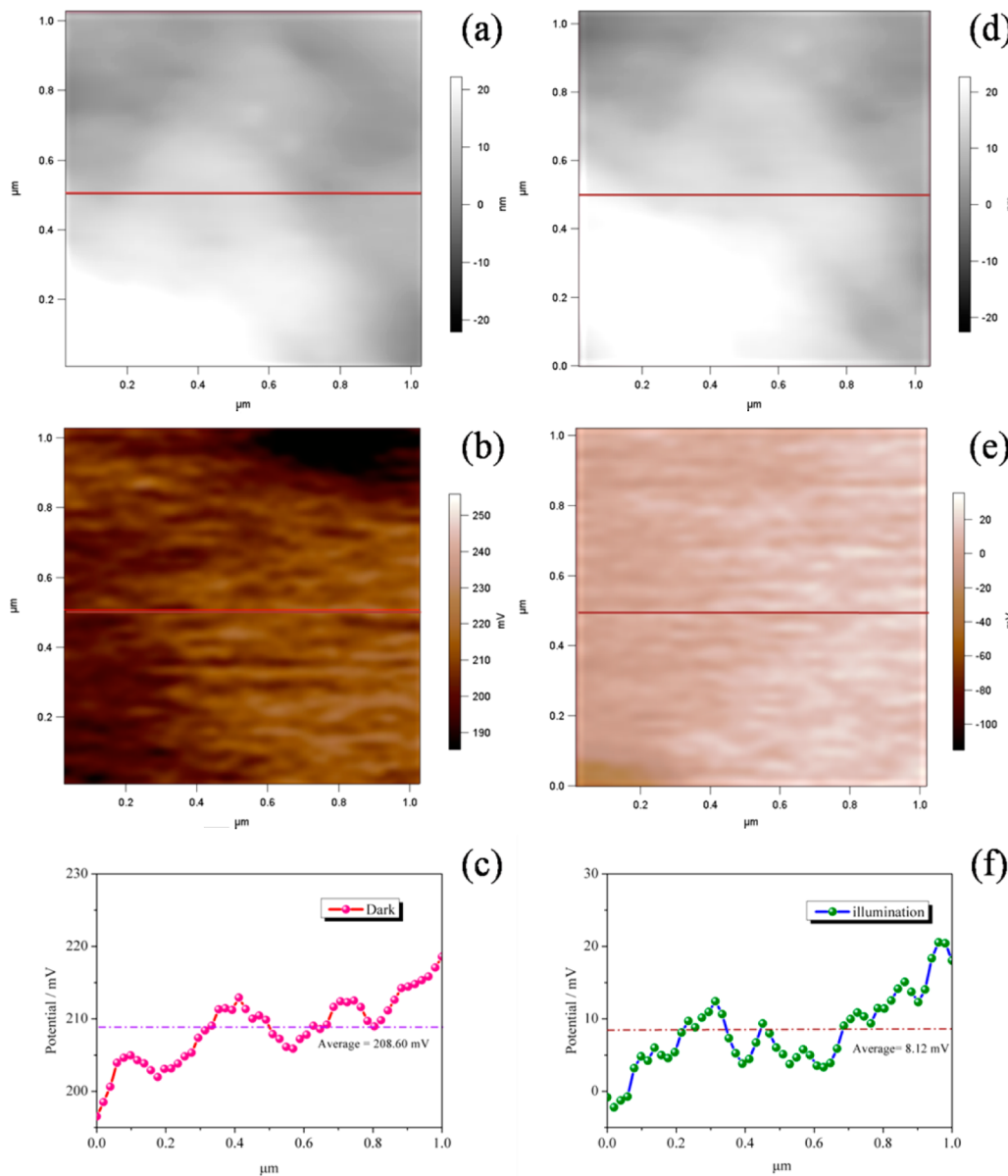


**Figure 4.** AFM (a,d), KPFM (b,e), and corresponding data curves (c,f) of the  $\text{CH}_3\text{NH}_3\text{PbBr}_3$  single crystal under dark and illumination.

room temperature. The obtained single crystal is a square cube with the size of  $14 \times 14 \text{ mm}$ . Photophysics performances of the sample on the spontaneous polarization, work function, as well as in situ generated current under dark and irradiation have been investigated.

The photograph of the as-prepared single crystal is displayed in Figure S1 in the SI. It was a cubic orange crystal with the size of about  $14 \times 14 \text{ mm}$ . Compared with the reported antisolvent vapor-assisted crystallization approach and top-seeded solution-growth method for hybrid perovskite single crystal,<sup>24,25</sup> there is plenty of superiorities about this method. In the preparation section, it can be seen that this method of facile-only single solvent is needed for the single crystal growth, with low demand for equipment; only a beaker is enough for the whole process, and there is no need to control temperature accurately. The sole key parameter is the concentration of the precursor solution.

The powder XRD patterns (Figure 1) for  $\text{MAPbBr}_3$  obtained from the solution reaction exhibit good agreement with the

calculated XRD patterns from the single-crystal models in Figure 2.

P\bar{4}3m (no. 215)，与报告结果一致。<sup>26-28</sup> 单晶X射线衍射数据和MAPbBr<sub>3</sub>的键长和键角在表S1和S2中给出。

通过PFM模式，我们测量了单晶的平面相(IPP)和非平面相(OPP)。图3中的OPP图像显示了增强的极化。具体来说，IPP和OPP图像(图3a,d)显示没有对应关系，表明极化较弱。相反，IPP和OPP图像(图3b,c)显示了规律的畴结构，表明极化在光照下更强。此外，可以发现OPP图像在光照条件下几乎没有变化。

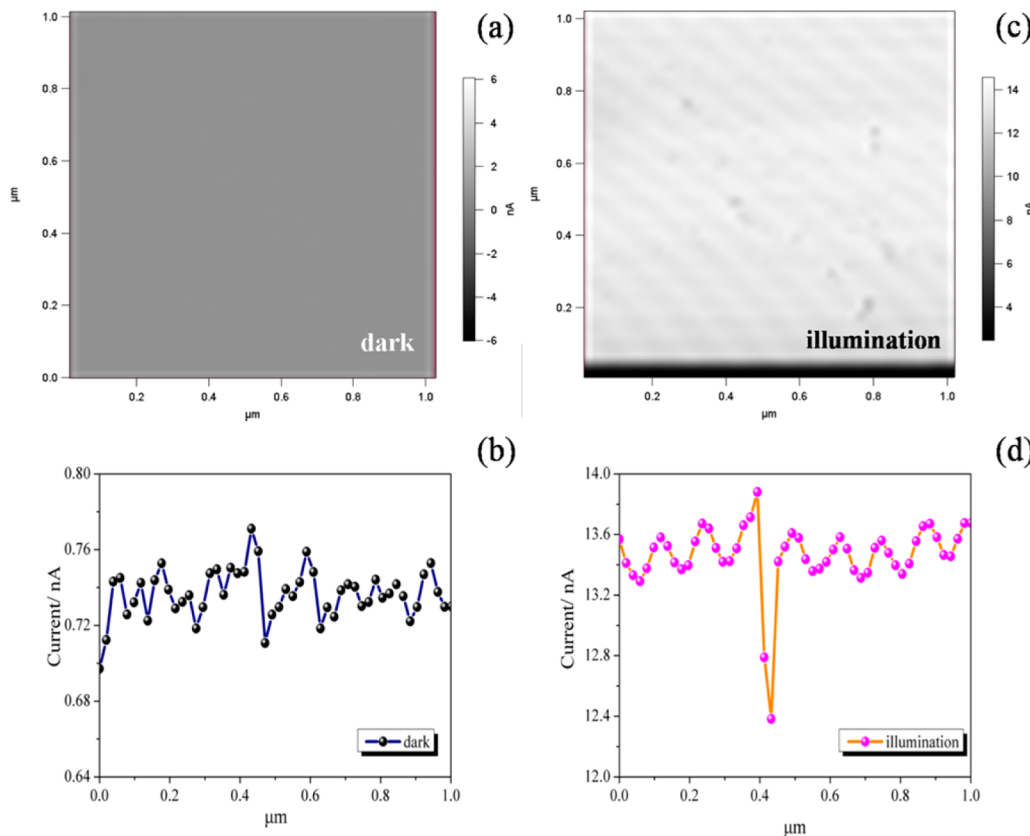


**Figure 5.** Surface current distribution (a,c) of  $\text{CH}_3\text{NH}_3\text{PbBr}_3$  single crystal under dark and illumination and the corresponding data profiles (b,d).

In general, the phase contrast in the PFM image suggests spontaneous polarization domains in ferroelectric materials. It has been demonstrated that the hybrid perovskite methylammonium lead iodide ( $\text{CH}_3\text{NH}_3\text{PbI}_3$ ) is ferroelectric at room temperature<sup>29–34</sup> due to the transport behavior of dipoles originated from its tetragonal phase.

The spontaneous polarization is very important, and it is usually used to explain the anomalous hysteresis in hybrid perovskite solar cells. Most recently, however, experimental and numerical simulations suggest that the observed so-called spontaneous polarization may be resulted of electrochemical phenomena, such as MA ionic migration and of the charge trapping.<sup>35,36</sup>

As for the  $\text{CH}_3\text{NH}_3\text{PbBr}_3$  single crystal, based on the fact that there are no polar cubic space groups, we believe that the observed “spontaneous polarization” phenomenon is also derived from carrier and ion transportation. The MA ions are rotationally mobile in perovskite crystal, which will give rise to local defects.

The data curves of IPP and OPP images are also displayed in Figure 3c,f. It is interesting to find that for both IPP and OPP the consistency of the phase angles improves a great deal when irradiation is added. This trend is particularly obvious for the IPP images. Under the dark condition, the phase angles are nearly random distribution, from  $-80$  to  $250^\circ$ ; on the contrary, the phase angle distribution is close to a straight line paralleled to the abscissa axis under illumination. It seems that the light is able to provide a tractive force to make the arrangement of the dipole convergent in bulk crystal. Although the intrinsic mechanism is unclear, this phenomenon is crucial to understand the photovoltaic performance of hybrid perovskite solar cells. Under illumination, mobile bromide vacancies and MA

ions migrate to opposite sides, and accumulation of those space charges induces electric fields. These built-in electric fields will display preferred orientation and accumulate. Thus, an extremely large open-circuit voltage will be generated. This is the well-known bulk photovoltaic effect (BPVE) in inorganic perovskite materials.<sup>37–39</sup>

On the basis of this phenomenon, we believe that the incident light mainly influences the transport behavior of MA ions along with the lateral direction.

Kelvin probe force microscopy (KPFM) is an in situ, contactless, and nondestructive technology to measure the surface potential of the sample. It has been one of the most powerful methods to investigate dynamics of surface charge on semiconductor materials. The charge-separation process consequently leads to a change in the surface potential of both surfaces with different signals. For photon-sensitized substance, the photogenerated charging and discharging processes can be detected by measuring the surface potential differences between dark and under illumination.

Figure 4 exhibits the AFM, KPFM images, and corresponding data curves of the  $\text{CH}_3\text{NH}_3\text{PbBr}_3$  single crystal under dark and illumination. Morphologies of the bulk single crystal before and after irradiation (Figure 4a,d) show smooth surface with a roughness of ca. 8 nm, and there is no visible difference between the two images, indicating that the light irradiation has no influence on the morphology.

However, on the other side, the surface potential images in Figure 4b,e present huge disparities on their contrasts. Under dark condition, the disparity between the KPFM tip and the sample was 190–200 mV, and the values decreased to  $-100$  to 20 mV when the single crystal was under illumination. The observed negative shift in the surface potential possibly implies

the hole accumulation within the  $\text{CH}_3\text{NH}_3\text{PbBr}_3$  bulk crystal with the injection of excitons into its conduction band. As a semiconductor, there is no generation of excess carriers under dark; however, because of depopulation of the energy states in the forbidden band gap under illumination, the photogenerated carriers quickly separated, creating a pool of excess holes on the surface of  $\text{CH}_3\text{NH}_3\text{PbBr}_3$ .<sup>40,41</sup>

For quantitative analysis, two data curves are shown in Figure 4c,f. It can be seen that the average disparity under dark was 208.60 mV and under illumination was 8.12 mV. This phenomenon expresses the fact that the bulk crystal's surface work function increases a great deal under illumination, and the disparity value can be calculated to be  $\Delta E \approx 200$  mV. This value is much larger than that of most oxide semiconductors. It is about 10 times larger than that of  $\text{TiO}_2$  (ca. 30 mV, under UV light)<sup>42</sup> and even larger than that of the quality epitaxial  $\text{BiFeO}_3$  films (0.16 V).<sup>43</sup> This large surface potential change may attribute to the light-enhanced polarization behavior in  $\text{CH}_3\text{NH}_3\text{PbBr}_3$  crystal under light, which has been previously discussed. When a photon is incident upon the top surface of  $\text{CH}_3\text{NH}_3\text{PbBr}_3$  bulk crystal, a hole-electron pair generated and then speedily separated to opposite directions, producing a gradient in the quasi-Fermi levels. Hence, a surface photo-voltage induces the surface photo potential.<sup>44</sup> This interpretation provides a rough mechanism about why the hybrid perovskite solar cells have larger open-circuit voltage than organic photovoltaics (OPVs) and dye-sensitized solar cells (DSSCs), especially the  $\text{CH}_3\text{NH}_3\text{PbBr}_3$ .

It should be noticed that these values were detected under a very weak irradiation ( $5 \text{ mW/cm}^2$ ). In general, this alteration would get larger when the illumination intensity increases.<sup>45,46</sup> It is reasonable to believe that the potential disparity value might be more arresting under AM 1.5 ( $100 \text{ mW/cm}^2$ ).

The surface distributions of current were also measured through the conductive AFM mode, which could provide the pictorial diagram about the current passing through the tip and the sample. The current mapping was presented in Figure 5a,c. Under both conditions, the currents are divided pretty much equally over the bulk crystal's surface. There is no sign for current attenuation at the entire measured region. On the contrary, the states of art of the hybrid perovskite solar cells are constructed based on polycrystalline films. In this state, the photogenerated current is always attenuated at the interface of grain boundaries due to grain potential barrier effect, making the real current density of the solar cells device much smaller than theoretical value.<sup>47,48</sup> Fortunately, there are minimal grains nor defects in single crystal, leading to the decreasing of carrier trap states. Consequently, the large-scale single crystal is expected to overcome this drawback and vastly improve device's photoelectric conversion efficiency. Moreover, data curves shows that the current magnitude in the dark was 0.7 nA, while this value increased to ca. 13.5 nA under light. The photogenerated current was  $\sim 20$  times larger than that of the dark one. To further confirm this, current-voltage curve is exhibited in Figure 6, and the scan range is from  $-10$  to  $+10$  V. Both characteristic curves reveal the typical Schottky contact feature. At the max positive bias of  $+10$  V, the current value was 0.67 nA for the dark and 11.79 nA for the illumination, which are in accordance with the surface current images.

In summary, a large-size methylammonium lead bromide hybrid perovskite single crystal with the dimension of 14  $\times$  14 mm has been prepared through a facile solution method at room temperature. By in situ investigation of the photophysics

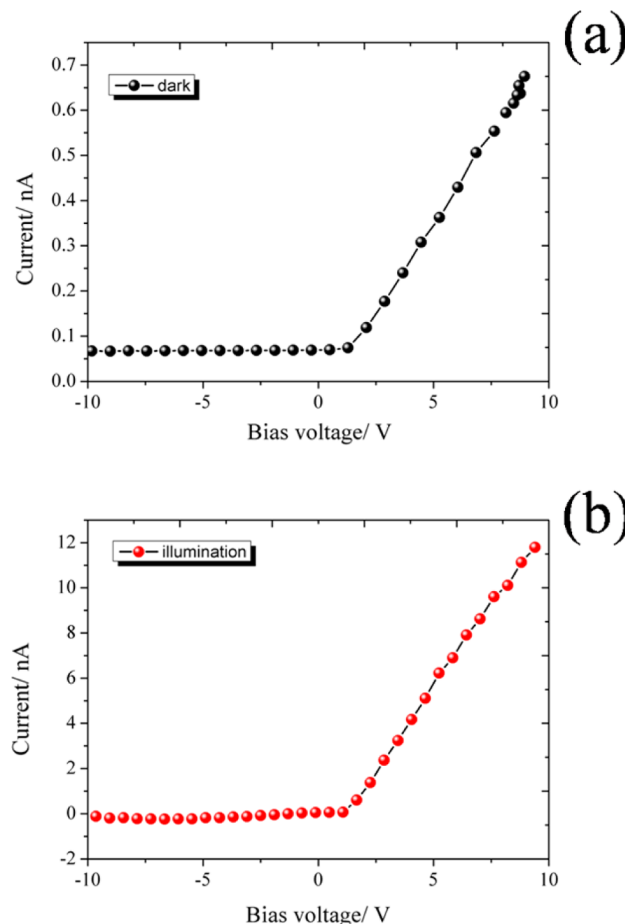


**Figure 6.** In situ  $I$ – $V$  curves of  $\text{CH}_3\text{NH}_3\text{PbBr}_3$  single crystal under dark and illumination.

properties under dark and irradiation, we have found the illumination is able to rearrange the PFM phase angles in bulk crystal and force them to become convergent. In addition, a large surface potential change of 200 mV was observed due to the accumulation of built-in potential fields in  $\text{CH}_3\text{NH}_3\text{PbBr}_3$  crystal under light. Photocurrents distributed equally over the crystal's surface and no current attenuation occurred in the entire measured region. The previously described features make the single-crystal devices have superior open-circuit voltage as well as electric current density compared with that of the polycrystalline film when it serves as light absorber in hybrid perovskite solar cells.

## ASSOCIATED CONTENT

### S Supporting Information

Details of experimental methods, digital photograph of as-prepared  $\text{CH}_3\text{NH}_3\text{PbBr}_3$  single crystal, crystallographic parameters obtained from single-crystal X-ray diffraction, and bond lengths for  $\text{MAPbBr}_3$ . The Supporting Information is available free of charge on the ACS Publications website at DOI: 10.1021/acs.jpclett.5b01017.

## AUTHOR INFORMATION

### Corresponding Authors

\*E-mail: xujb@ms.xjb.ac.cn (J.X.).

\*E-mail: renw@ms.xjb.ac.cn (W.R.).

### Notes

The authors declare no competing financial interest.

## ACKNOWLEDGMENTS

This work was supported by the West Light Foundation of The Chinese Academy of Sciences (no. XBBS-2014-04, no. RCPY201206), and the 1000-Talent Program (Recruitment Program of Global Expert), and National Natural Science Foundation of China (41130746 and 41302029), and International Technology Cooperation Foundation of Autonomous Region (20136009), and the Director Foundation of XTIPC, CAS (No. 2015RC010).

## REFERENCES

- (1) Espinosa, N.; Serrano-Luján, L.; Urbin, A.; Krebs, F. C. Solution and Vapour Deposited Lead Perovskite Solar Cells: Ecotoxicity from a Life Cycle Assessment Perspective. *Sol. Energy Mater. Sol. Cells* **2015**, *137*, 303–310.
- (2) Park, N. G. Organometal Perovskite Light Absorbers Toward a 20% Efficiency Low-Cost Solid-State Mesoscopic Solar Cell. *J. Phys. Chem. Lett.* **2013**, *4*, 2423–2429.
- (3) Kamat, P. V. Emergence of New Materials for Light –Energy Conversion: Perovskites, Metal Clusters, and 2-D Hybrids. *J. Phys. Chem. Lett.* **2014**, *5*, 4167–4168.
- (4) Green, M. A.; Emery, K.; Hishikawa, Y.; Warta, W.; Dunlop, E. D. Solar Cell Efficiency Tables (Version 45). *Prog. Photovoltaics* **2015**, *23*, 1–9.
- (5) Park, N. G. Switchable Photovoltaics. *Nat. Mater.* **2015**, *14*, 140–141.
- (6) Stranks, S. D.; Eperon, G. E.; Grancini, G.; Menelaou, C.; Alcocer, M. J. P.; Leijtens, T.; Herz, L. M.; Petrozza, A.; Snaith, H. J. Electron-Hole Diffusion Lengths Exceeding 1 Micrometer in an Organometal Trihalide Perovskite Absorber. *Science* **2013**, *342*, 341–344.
- (7) Xing, G.; Mathews, N.; Sun, S.; Lim, S. S.; Lam, Y. M.; Grätzel, M.; Mhaisalkar, S.; Sum, T. C. Long-Range Balanced Electron and Hole-Transport Lengths in Organic-Inorganic  $\text{CH}_3\text{NH}_3\text{PbI}_3$ . *Science* **2013**, *342*, 344–347.
- (8) Hodes, G. Perovskite-Based Solar Cells. *Science* **2013**, *342*, 317–318.
- (9) Wang, S.; Ono, L. K.; Leyden, M. R.; Kato, Y.; Raga, S. R.; Lee, M. V.; Qi, Y. Smooth Perovskite Thin Films and Efficient Perovskite Solar Cells Prepared by the Hybrid Deposition Method. *J. Mater. Chem. A* **2015**, DOI: 10.1039/C5TA03593G.
- (10) Koh, T. M.; Fu, K.; Fang, Y.; Chen, S.; Sum, T. C.; Mathews, N.; Mhaisalkar, S. G.; Boix, P. P.; Baikie, T. Formamidinium-Containing Metal-Halide: An Alternative Material for Near-IR Absorption Perovskite Solar Cells. *J. Phys. Chem. C* **2014**, *118*, 16458–16462.
- (11) Lv, S.; Pang, S.; Zhou, Y.; Padture, N. P.; Hu, H.; Wang, L.; Zhou, X.; Zhu, H.; Zhang, L.; Huang, C.; et al. One-step, Solution-processed Formamidinium Lead Trihalide ( $\text{FAPbI}_{(3-x)}\text{Cl}_x$ ) for Mesoscopic Perovskite–polymer Solar Cells. *Phys. Chem. Chem. Phys.* **2014**, *16*, 19206–19211.
- (12) Yin, W. J.; Yang, J. H.; Kang, J.; Yan, Y.; Wei, S. H. Halide Perovskite Materials for Solar Cells: A Theoretical Review. *J. Mater. Chem. A* **2015**, *3*, 8926–8942.
- (13) Hao, F.; Stoumpos, C. C.; Cao, D. H.; Chang, R. P. H.; Kanatzidis, M. G. Lead-free Solid-state Organic–inorganic Halide Perovskite Solar Cells. *Nat. Photonics* **2014**, *8*, 489–494.
- (14) Umari, P.; Mosconi, E.; Angelis, F. D. Relativistic GW Calculations on  $\text{CH}_3\text{NH}_3\text{PbI}_3$  and  $\text{CH}_3\text{NH}_3\text{SnI}_3$  Perovskites for Solar Cell Applications. *Sci. Rep.* **2014**, *4*, 4467.
- (15) Liu, M.; Johnston, M. B.; Snaith, H. J. Efficient Planar Heterojunction Perovskite Solar Cells by Vapour Deposition. *Nature* **2013**, *501*, 395–398.
- (16) Chen, Q.; Zhou, H.; Hong, Z.; Luo, S.; Duan, H. S.; Wang, H. H.; Liu, Y.; Li, G.; Yang, Y. Planar Heterojunction Perovskite Solar Cells via Vapor-Assisted Solution Process. *J. Am. Chem. Soc.* **2013**, *136*, 622–625.
- (17) Edri, E.; Kirmayer, S.; Henning, A.; Mukhopadhyay, S.; Gartsman, K.; Rosenwaks, Y.; Hodes, G.; Cahen, D. Why Lead Methylammonium Tri-Iodide Perovskite-Based Solar Cells Require a Mesoporous Electron Transporting Scaffold (but Not Necessarily a Hole Conductor). *Nano Lett.* **2014**, *14*, 1000–1004.
- (18) Tan, K. W.; Moore, D. T.; Saliba, M.; Sai, H.; Estroff, L. A.; Hanrath, T.; Snaith, H. J.; Wiesner, U. Thermally Induced Structural Evolution and Performance of Mesoporous Block Copolymer-Directed Alumina Perovskite Solar Cells. *ACS Nano* **2014**, *8*, 4730–4739.
- (19) Nie, W.; Tsai, H.; Asadpour, R.; Blancon, J. C.; Amanda, J. N.; Gupta, G.; Crochet, J. J.; Chhowalla, M.; Tretiak, S.; Alam, M. A.; et al. High-efficiency Solution-processed Perovskite Solar Cells with Millimeter-scale Grains. *Science* **2015**, *347*, 522–525.
- (20) Shi, D.; Adinolfi, V.; Comin, R.; Yuan, M.; Alarousu, E.; Buin, A.; Chen, Y.; Hoogland, S.; Rothenberger, A.; Katsiev, K.; et al. Low Trap-state Density and Long Carrier Diffusion in Organolead Trihalide Perovskite Single Crystals. *Science* **2015**, *347*, 519–522.
- (21) Dong, Q.; Fang, Y.; Shao, Y.; Mulligan, P.; Qiu, J.; Cao, L.; Huang, J. Electron-hole Diffusion Lengths >175  $\mu\text{m}$  in Solution-grown  $\text{CH}_3\text{NH}_3\text{PbI}_3$  Single Crystals. *Science* **2015**, *347*, 967–970.
- (22) Dang, Y.; Liu, Y.; Sun, Y.; Yuan, D.; Liu, X.; Lu, W.; Liu, G.; Xia, H.; Tao, X. Bulk Crystal Growth of Hybrid Perovskite Material  $\text{CH}_3\text{NH}_3\text{PbI}_3$ . *CrystEngComm* **2015**, *17*, 665–670.
- (23) Baikie, T.; Fang, Y.; Kadro, J. M.; Schreyer, M.; Wei, F.; Mhaisalkar, S. G.; Graetzel, M.; White, T. J. Synthesis and Crystal Chemistry of the Hybrid Perovskite  $(\text{CH}_3\text{NH}_3)\text{PbI}_3$  for Solid-state Sensitised Solar Cell Applications. *J. Mater. Chem. A* **2013**, *1*, 5628–5641.
- (24) Fang, H. H.; Raissa, R.; Abdu-Aguye, M.; Adjokatse, S.; Blake, G. R.; Even, J.; Loi, M. A. Photophysics of Organic–Inorganic Hybrid Lead Iodide Perovskite Single Crystals. *Adv. Funct. Mater.* **2015**, *25*, 2378–2385.
- (25) Mashiyama, H.; Kawamura, Y.; Kasano, H.; Asahi, T.; Noda, Y.; Kimura, H. Disordered Configuration of Methylammonium of  $\text{CH}_3\text{NH}_3\text{PbBr}_3$  Determined by Single Crystal Neutron Diffractometry. *Ferroelectrics* **2007**, *348*, 182–186.
- (26) Schmidt, L. C.; Pertegás, A.; Carrero, S. G.; Malinkiewicz, O.; Agouram, S.; Espallargas, G. M.; Bolink, H. J.; Galian, R. E.; Prieto, J. P. Nontemplate Synthesis of  $\text{CH}_3\text{NH}_3\text{PbBr}_3$  Perovskite Nanoparticles. *J. Am. Chem. Soc.* **2014**, *136*, 850–853.
- (27) Mashiyama, H.; Kawamura, Y.; Kubota, Y. The Anti-Polar Structure of  $\text{CH}_3\text{NH}_3\text{PbBr}_3$ . *J. Korean Phys. Soc.* **2007**, *51*, 850–853.
- (28) Sadhanala, A.; Deschler, F.; Thomas, T. H.; Dutton, S. E.; Goedel, K. C.; Hanusch, F. C.; Lai, M. L.; Steiner, U.; Bein, T.; Docampo, P.; et al. Preparation of Single-Phase Films of  $\text{CH}_3\text{NH}_3\text{Pb}(\text{II}-x\text{Br}_x)_3$  with Sharp Optical Band Edges. *J. Phys. Chem. Lett.* **2014**, *5*, 2501–2505.
- (29) Wei, J.; Zhao, Y.; Li, H.; Li, G.; Pan, J.; Xu, D.; Zhao, Q.; Yu, D. Hysteresis Analysis Based on the Ferroelectric Effect in Hybrid Perovskite Solar Cells. *J. Phys. Chem. Lett.* **2014**, *5*, 3937–3945.
- (30) Fan, Z.; Xiao, J.; Sun, K.; Chen, L.; Hu, Y.; Ouyang, J.; Ong, K. P.; Zeng, K.; Wang, J. Ferroelectricity of  $\text{CH}_3\text{NH}_3\text{PbI}_3$  Perovskite. *J. Phys. Chem. Lett.* **2015**, *6*, 1155–1161.
- (31) Kutes, Y.; Ye, L.; Zhou, Y.; Pang, S.; Huey, B. D.; Padture, N. P. Direct Observation of Ferroelectric Domains in Solution-Processed  $\text{CH}_3\text{NH}_3\text{PbI}_3$  Perovskite Thin Films. *J. Phys. Chem. Lett.* **2014**, *5*, 3335–3339.
- (32) Zhao, P.; Xu, J.; Ma, C.; Ren, W.; Wang, L.; Bian, L.; Chang, A. Spontaneous Polarization Behaviors in Hybrid Halide Perovskite Film. *Scr. Mater.* **2015**, *102*, 51–54.
- (33) Chen, H. W.; Sakai, N.; Ikegam, M.; Miyasaka, T. Emergence of Hysteresis and Transient Ferroelectric Response in Organo-Lead Halide Perovskite Solar Cells. *J. Phys. Chem. Lett.* **2015**, *6*, 164–169.
- (34) Liu, S.; Zheng, F.; Koocher, N. Z.; Takenaka, H.; Wang, F.; Rappe, A. M. Ferroelectric Domain Wall Induced Band Gap Reduction and Charge Separation in Organometal Halide Perovskites. *J. Phys. Chem. Lett.* **2015**, *6*, 693–699.

- (35) Beilsten-Edmands, J.; Eperon, G. E.; Johnson, R. D.; Snaith, H. J.; Radelli, P. G. Non-ferroelectric Nature of the Conductance Hysteresis in  $\text{CH}_3\text{NH}_3\text{PbI}_3$  Perovskite-based Photovoltaic Devices. *Appl. Phys. Lett.* **2015**, *106*, 173502.
- (36) Frost, M. J.; Butler, T. K.; Walsh, A. Molecular ferroelectric contributions to anomalous hysteresis in hybrid perovskite solar cells. *APL Mater.* **2014**, *2*, 081506.
- (37) Ji, W.; Yao, K.; Liang, Y. C. Bulk Photovoltaic Effect at Visible Wavelength in Epitaxial Ferroelectric  $\text{BiFeO}_3$  Thin Films. *Adv. Mater.* **2010**, *22*, 1763–1766.
- (38) Yang, S. Y.; Seidel, J.; Byrnes, S. J.; Shafer, P.; Yang, C. H.; Rossell, M. D.; Yu, P.; Chu, Y. H.; Scott, J. F.; Ager, J. W.; et al. Above-bandgap Voltages from Ferroelectric Photovoltaic Devices. *Nat. Nanotechnol.* **2010**, *5*, 143–147.
- (39) Butler, T. K.; Frost, M. J.; Walsh, A. Ferroelectric Materials for Solar Energy Conversion: Photoferroics Revisited. *Energy Environ. Sci.* **2015**, *8*, 838–848.
- (40) Johnson, F.; Song, S. H.; Abrahamson, J.; Liptak, R.; Aydil, E.; Campbell, S. A. Sputtered Metal Oxide Broken Gap Junctions for Tandem Solar Cells. *Sol. Energy Mater. Sol. Cells* **2015**, *132*, 515–522.
- (41) Li, S.; Chen, C. W. Polymer-metal-oxide Hybrid Solar Cells. *J. Mater. Chem. A* **2013**, *1*, 10574–10591.
- (42) Ikeda, M.; Koide, N.; Han, L.; Sasahara, A.; Onishi, H. Work Function on Dye-Adsorbed  $\text{TiO}_2$  Surfaces Measured by Using a Kelvin Probe Force Microscope. *J. Phys. Chem. C* **2008**, *112*, 6961–6967.
- (43) Yan, F.; Chen, G.; Lu, Li; Spanier, J. E. Dynamics of Photogenerated Surface Charge on  $\text{BiFeO}_3$  Films. *ACS Nano* **2012**, *6*, 2353–2360.
- (44) Fan, X.; Zang, L.; Zhang, M.; Qiu, H.; Wang, Z.; Yin, J.; Jia, H.; Pan, S.; Wang, C. A Bulk Boron-Based Photocatalyst for Efficient Dechlorination:  $\text{K}_3\text{B}_6\text{O}_{10}\text{Br}$ . *Chem. Mater.* **2014**, *26*, 3169–3174.
- (45) Liu, C.; Hwang, Y. J.; Jeong, H. E.; Yang, P. Light-Induced Charge Transport Within A Single Asymmetric Nanowire. *Nano Lett.* **2011**, *11*, 3755–3758.
- (46) Yoo, H.; Bae, C.; Yang, Y.; Lee, S.; Kim, M.; Kim, H.; Kim, Y.; Shin, H. Spatial Charge Separation in Asymmetric Structure of Au Nanoparticle on  $\text{TiO}_2$  Nanotube by Light-Induced Surface Potential Imaging. *Nano Lett.* **2014**, *14*, 4413–4417.
- (47) Dymshits, A.; Henning, A.; Segev, G.; Rosenwaks, Y.; Etgar, L. The Electronic Structure of Metal Oxide/Organo Metal Halide Perovskite Junctions in Perovskite Based Solar Cells. *Sci. Rep.* **2015**, *5*, 8704.
- (48) Hurtley, S. Large-Crystal Perovskite Films. *Science* **2015**, *347*, 517–B.